Article

# Methylrhenium Trioxide Revisited: Mechanisms for Nonredox Oxygen Insertion in an M–CH Bond

Jason M. Gonzales, Robert Distasio, Roy A. Periana, William A. Goddard, and Jonas Oxgaard

*J. Am. Chem. Soc.*, **2007**, 129 (51), 15794-15804 • DOI: 10.1021/ja0714742



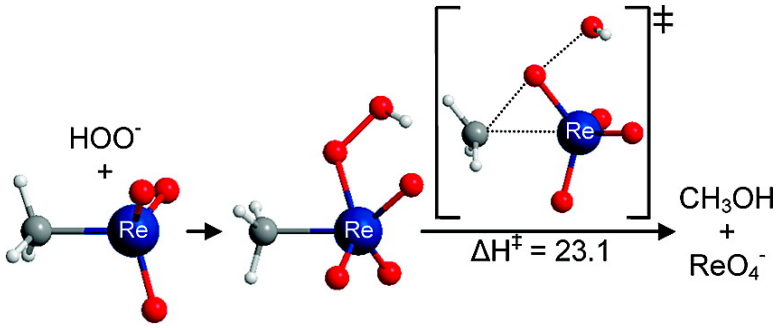


## More About This Article

Additional resources and features associated with this article are available within the HTML version:

- Supporting Information
- Links to the 4 articles that cite this article, as of the time of this article download
- Access to high resolution figures
- Links to articles and content related to this article
- Copyright permission to reproduce figures and/or text from this article

View the Full Text HTML

J|A|C|S
ARTICLES
Published on Web 12/04/2007

# Methylrhenium Trioxide Revisited: Mechanisms for Nonredox Oxygen Insertion in an M−$CH_3$ Bond

Jason M. Gonzales,† Robert Distasio Jr.,† Roy A. Periana,*,‡ William A. Goddard III,*,† and Jonas Oxgaard*,†

*Contribution from the Materials and Process Simulation Center, Beckman Institute (139-79), Division of Chemistry and Chemical Engineering, California Institute of Technology, Pasadena, California 91125, and The Scripps Research Institute, Scripps Florida, 5353 Parkside Drive, Bldg T2, Office 205, Jupiter, Florida 33458*

Received March 2, 2007; E-mail: rperiana@scripps.edu; wag@wag.caltech.edu; oxgaard@wag.caltech.edu

***Abstract:*** Methylrhenium trioxide (**MTO**) has the rare ability to stoichiometrically generate methanol at room temperature with an external oxidant ($H_2O_2$) under basic conditions. In order to use this transformation as a model for nonredox oxidative C−O coupling, the mechanisms have been elucidated using density functional theory (DFT). Our studies show several possible reaction pathways to form methanol, with the lowest net barrier ($\Delta H^{\ddagger}$) being 23.3 kcal $mol^{-1}$. The rate-determining step is a direct "Baeyer−Villiger" type concerted oxygen insertion into **MTO**, forming methoxyrhenium trioxide. The key to the low-energy transition state is the donation of electron density, first, from HOO(−) to the $-CH_3$ group (making $-CH_3$ more nucleophilic and HOO− more electrophilic) and, second, from the Re−C bond to both the forming Re−O and breaking O−O bonds, simultaneously (thus forming the Re−O bond as the Re−C bond is broken). In turn, the ability of MTO to undergo these transfers can be traced to the electrophilic nature of the metal center and to the absence of accessible d-orbitals. If accessible d-orbitals are present, they would most likely donate the required electron density instead of the M−$CH_3$ moiety, and this bond would thus not be broken. It is possible that other metal centers with similar qualities, such as $Pt^{IV}$ or $Ir^{V}$, could be competent for the same type of chemistry.

## Introduction

The chemical energy stored in the world's resources of methane is comparable to that of petroleum, but the vast majority of this methane is grossly underutilized (often flared). This is mainly due to the prohibitive economics of transporting a gas with a low value per cubic meter, something that could be vastly improved by the development of an efficient low-temperature catalytic process to convert the methane to liquid forms (e.g., methanol). However, despite extensive effort,[1−12] this has not yet been realized, mainly due to the complexity involved in selectively activating the relatively inert methane C−H bond, and then selectively functionalizing the methyl intermediate through C−O bond formation.

While neither of these two steps is trivial by themselves, there also appears to be a dichotomy between what conditions enable them. Thus, C−H activation is normally carried out by early metal $d^0$ complexes or late metal complexes in low oxidation states ($Ir^{I}$, $Ir^{III}$, $Ru^{II}$, $Os^{II}$), while C−O functionalization is normally carried out by late metals in relatively high oxidation states ($Pd^{II}/Pd^{IV}$, $Pt^{II}/Pt^{IV}$, $Au^{III}$, $Hg^{II}$). Thus, a plausible reason for the dearth of bifunctional catalysts is that C−H activation and C−O coupling require different and possibly mutually exclusive conditions, and to successfully design a bifunctional system requires a significantly increased understanding of the factors underlying these two processes.

One of the more interesting systems for this purpose is methylrhenium trioxide ($CH_3ReO_3$, **MTO**). **MTO** is a versatile catalyst for a wide variety of oxygen transfer reactions, due to its ability to donate an oxygen atom to various substrates.[13−24]

† California Institute of Technology.
‡ The Scripps Research Institute.

(1) Crabtree, R. H. *Chem. Rev.* **1995**, *95*, 987.
(2) Shilov, A. E.; Shul'pin, G. B. *Chem. Rev.* **1997**, *97*, 2879.
(3) Derouane, E. G.; Haber, J.; Lemos, F.; Ribeiro, F.; Guisnet, M. *Catalytic Activation and Functionalization of Light Alkanes - Advances and Challenges*; Kluwer Academic Publishers: Norwell, MA, 1998.
(4) Strassner, T.; Muehlhofer, M.; Zeller, A.; Herdtweck, E.; Hermann, W. A. *J. Organomet. Chem.* **2004**, *689*, 1418.
(5) Periana, R. A.; Miranov, O.; Taube, D. J.; Bhalla, G.; Jones, C. *Science* **2003**, *301*, 814.
(6) Periana, R. A.; Taube, D. J.; Gamble, S.; Taube, H.; Satoh, T.; Fuji, H. *Science* **1998**, *280*, 560.
(7) Kua, J.; Xu, X.; Periana, R. A.; Goddard, W. A., III. *Organometallics* **2002**, *21*, 511.
(8) Xu, X.; Kua, J.; Periana, R. A.; Goddard, W. A., III. *Organometallics* **2003**, *22*, 2057.
(9) Jones, C.; Taube, D.; Ziatdinov, V. R.; Periana, R. A.; Nielsen, R. J.; Oxgaard, J.; Goddard, W. A., III. *Angew. Chem., Int. Ed.* **2004**, *43*, 2.
(10) Lin, M.; Hogan, T.; Sen, A. *J. Am. Chem. Soc.* **1997**, *119*, 6048.
(11) Lin, M.; Hogan, T.; Sen, A. *J. Am. Chem. Soc.* **1996**, *118*, 4574.
(12) Periana, R. A.; Taube, D. J.; Evitt, E. R.; Loffler, D. G.; Wentrcek, P. R.; Voss, G.; Masuda, T. *Science* **1993**, *259*, 340.
(13) Stankovic, S.; Espenson, J. H. *J. Org. Chem.* **2000**, *65*, 5528.
(14) Adam, W.; Saha-Möller, C. R.; Weichold, O. *J. Org. Chem.* **2000**, *65*, 2897.
(15) Wang, Y.; Espenson, J. H. *J. Org. Chem.* **2000**, *65*, 104.
(16) Saladino, R.; Neri, V.; Cardona, F.; Goti, A. *Adv. Synth. Catal.* **2004**, *346*, 639.
(17) Santos, A. M.; Pedro, F. M.; Yogalekar, A. A.; Lucas, I. S.; Romão, C. C.; Kühn, F. E. *Chem.—Eur. J.* **2004**, *10*, 6313.
(18) Zauche, T. H.; Espenson, J. H. *Inorg. Chem.* **1998**, *37*, 6827.
(19) Owens, G. S.; Arias, J.; Abu-Omar, M. M. *Catal. Today* **2000**, *55*, 317.
(20) Kaple, K. P. In *Advances in Organometallic Chemistry*; Academic Press Inc.: San Diego, CA, 1997; Vol. 41, p 127.
(21) Herrmann, W. A.; Kühn, F. E. *Acc. Chem. Res.* **1997**, 30, 169.


**10.1021/ja0714742 CCC: $37.00** 

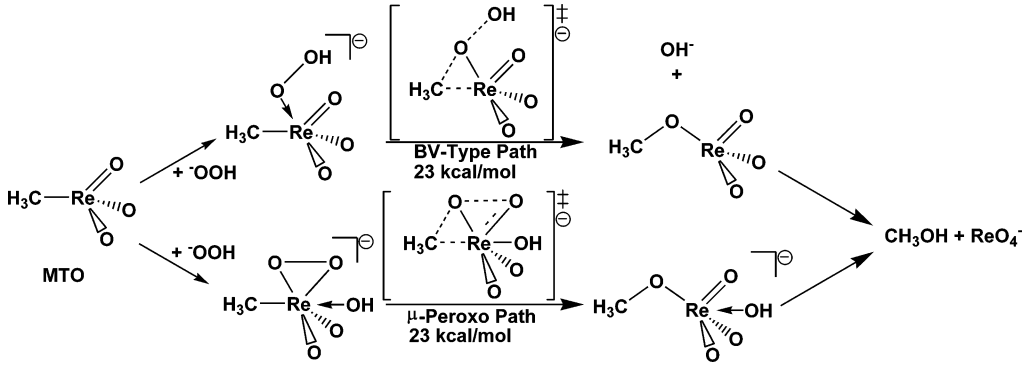


***Figure 1.*** Summary of preliminary work in ref 33.

Herrmann et al.[25] observed that exposing **MTO** to hydrogen peroxide under neutral conditions leads to a series of $\mu$-peroxo species and, under basic conditions, yields a perrhenate ion ($ReO_4^-$). Later analysis showed that stoichiometric amounts of methanol forms along with perrhenate, in addition to trace amounts of methane.[26−32] The formation of perrhenate and methanol is normally unwanted, as it destroys the catalyst, but it occurred to us that this is a rare example of a facile, room-temperature C−O coupling reaction from an M−$CH_3$ species and could thus be seen as a model for other C−O functionalization systems. Furthermore, as the Re is in the Re(VII) oxidation state and is thus a $d^0$ metal, it also occurred to us that the functionalization mechanism here should not be a redox mechanism, which could open up entirely new pathways for bifunctional catalyst systems.

Consequently, we initiated a joint experimental/computational mechanistic study of the reaction between **MTO** and $H_2O_2$/NaOH in THF[33] and have reported on preliminary results where we concluded that there are two main pathways (see Figure 1). The first pathway (Figure 1, top) proceeds through a transition state reminiscent of that in the organic Baeyer−Villiger (BV) reaction, that is, insertion of the oxygen into the C−Re bond with a concerted departure of the leaving group $OH^-$, with a barrier of 23 kcal $mol^{-1}$. The second pathway (Figure 1, bottom) went through an associative transition state, in which the oxidant first forms a $\mu$-peroxo species with a coordinating hydroxide ion. This undergoes an internal rearrangement where the O−O bond is broken as the C−O bond is formed, with a barrier of 18 kcal $mol^{-1}$. Based on these mechanisms, we postulated that several additional oxygen donors (including $ON(CH_3)_3$, PyO, DMSO, $IO_4^-$, and PhIO) should be competent for this chemistry, which was confirmed by both theory and experiment.[33]

***Scheme 1***

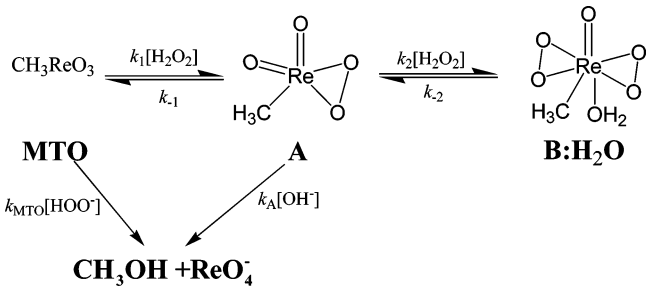


We now report on the full mechanistic investigation of these interactions, with an in-depth analysis of the key transition states for oxygen insertion into the M−$CH_3$ bond and the factors that enable them. We also analyze the mechanisms responsible for the formation of the mono- and di-$\mu$-peroxo species from the reaction of **MTO** and $H_2O_2$ in neutral environments, as well as the careful description of the complicated series of reactions connecting **MTO** and the peroxo species with methanol, which can occur via several different oxygen insertion transition states.

## Background

Under neutral conditions, **MTO** reacts with hydrogen peroxide to form two peroxo−rhenium complexes with 1:1 and 2:1 peroxide/rhenium ratios (see Scheme 1).[25] Note that the di-$\mu$-peroxo species, **B:$H_2O$**, is stabilized with one bound water, which is not the case with the $\mu$-peroxo species, **A**. Under basic conditions MTO and peroxide react to form perrhenate ($ReO_4^-$) and methanol. The noncatalytic reactions of **MTO** have been explored by numerous groups.[15,16,26,28,34−44] in a number of different systems, with the definitive work focusing entirely on the solvolytic reactions of **MTO** and $H_2O_2$ in tetrahydrofuran.[26] In this work Espenson and his colleagues expanded upon the solvolytic reactions by also considering the decomposition

(22) Kühn, F. E.; Herrmann, W. A. In *Structure and Bonding*; Meunier, B., Ed.; Springer-Verlag: Heidelberg, Berlin, 2000; Vol. 97, p 213.
(23) Mathew, T. M.; du Plessis, A. J. K.; Prinsloo, J. J. *J. Mol. Catal. A* **1999**, *148*, 157.
(24) Kühn, F. E.; Scherbaum, A.; Herrmann, W. A. *J. Organomet. Chem.* **2004**, *689*, 4149.
(25) Herrmann, W. A.; Fischer, R. W.; Marz, D. W. *Angew. Chem., Int. Ed. Engl.* **1991**, *30*, 1638.
(26) Abu-Omar, M. M.; Hansen, P. J.; Espenson, J. H. *J. Am. Chem. Soc.* **1996**, *118*, 4966.
(27) Espenson, J. H.; Tan, H.; Houk, R. S.; Eager, M. D. *Inorg. Chem.* **1998**, *37*, 4621.
(28) Wang, W.; Espenson, J. H. *J. Am. Chem. Soc.* **1998**, *120*, 11335.
(29) Pestovsky, O.; van Eldik, R.; Huston, P.; Espenson, J. H. *J. Chem. Soc., Dalton Trans.* **1995**, 133.
(30) Yamazaki, S.; Espenson, J. H.; Huston, P. *Inorg. Chem.* **1993**, *32*, 4683.
(31) Adolfsson, H.; Copéret, C.; Chiang, J. P.; Yudin, A. K. *J. Org. Chem.* **2000**, *65*, 8561.
(32) Herrmann, W. A.; Fischer, R. W.; Rauch, M. U.; Scherer, W. *J. Mol. Catal.* **1994**, *86*, 243.
(33) Conley, B. L.; Gonzales, J. M.; Ganesh, S. K.; Tenn, W. J., III; Young, K. J. H.; Oxgaard, J.; Goddard, W. A., III; Periana, R. A. *J. Am. Chem. Soc.* **2006**, *128*, 9018.
(34) Huang, R.; Espenson, J. H. *J. Org. Chem.* **1999**, *64*, 6374.
(35) Lahti, D. W.; Espenson, J. H. *Inorg. Chem.* **2000**, *39*, 2164.
(36) Stankovic, S.; Espenson, J. H. *J. Org. Chem.* **1998**, *63*, 4129.
(37) Tan, H.; Yoshikawa, A.; Gordon, M. S.; Espenson, J. H. *Organometallics* **1999**, *18*, 4753.
(38) Espenson, J. H.; Zhu, Z.; Zauche, T. H. *J. Org. Chem.* **1999**, *64*, 1191.
(39) Stankovic, S.; Espenson, J. H. *J. Org. Chem.* **2000**, *65*, 2218.
(40) Tetzlaff, H. R.; Espenson, J. H. *Inorg. Chem.* **1999**, *38*, 881.
(41) Villa de P, A. L.; De Vos, D. E.; Montes de C, C.; Jacobs, P. A. *Tetrahedron Lett.* **1998**, *39*, 8521.
(42) Wu, Y.; Sun, J. *J. Org. Chem.* **1998**, *63*, 1752.
(43) Owens, G. S.; Durazo, A.; Abu-Omar, M. M. *Chem.—Eur. J.* **2002**, *8*, 3053.
(44) Arends, I. W. C. E.; Sheldon, R. A. *Top. Catal.* **2002**, *19*, 133.

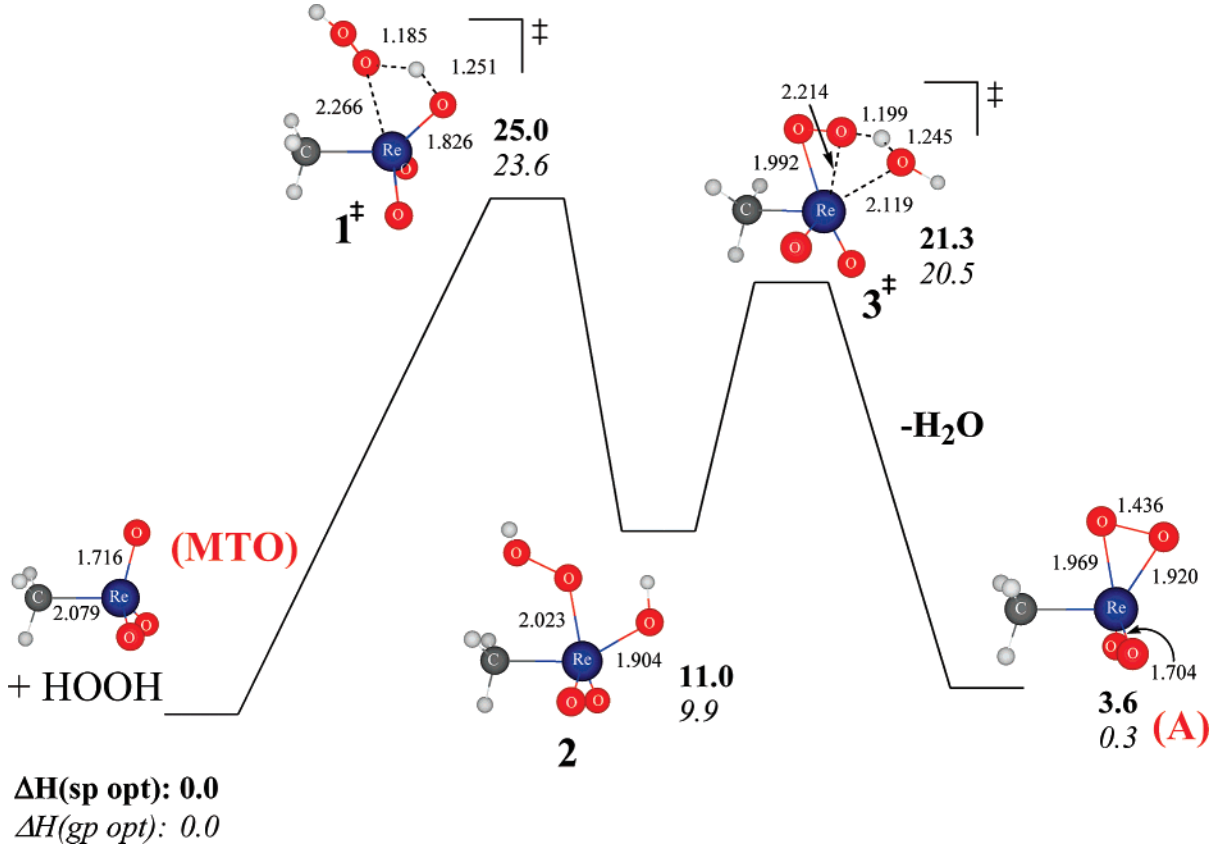


***Figure 2.*** Reaction profile of **MTO** + $H_2O_2$ → **A** + $H_2O$. The top numbers are enthalpies from solution-phase optimized structures, while the italicized bottom numbers are enthalpies using gas-phase structures with single-point solvation corrections. All energies are with respect to **MTO** and $H_2O_2$ and are listed in kcal mol$^{-1}$, and all distances are listed in Å.

reactions of MTO in basic environments, considering the kinetics and mechanisms of methanol and the perrhenate anion formation.

Espenson's kinetic work was quite detailed, and he and his collaborators explored the kinetics of the four above reactions using numerous experimental techniques, but primarily due to fast isotopic switching, he was not able to address a few key points. These include details on the mechanisms of each of the four reactions (several were proposed, but not actually confirmed) as well as the barriers associated with each step. Of particular interest is the relative ordering of the barriers under basic conditions, namely **MTO** + $OOH^-$ and **A** + $OH^-$. These two reactions have the same type of rate expression, and isotope labeling studies were unable to differentiate between them due to very fast oxygen exchange between the product perrhenate anion ($ReO_4^-$) and water.

In addition to the seminal work by Espenson et al., Sharpless and co-workers studied the decomposition of **MTO** in the presence of substituted pyridines[45,46] and found that while epoxidation rates were increased with the addition of pyridines, so were the decomposition rates. However, a balance could be found by using less basic pyridines, such as cyano-pyridine. Moreover, several theoretical investigations on the geometry and electronic structure of the **MTO** ground state have appeared.[47−51] The most relevant result for this investigation is the observation that the Re center is surprisingly electron-rich for a $d^0$ metal, due to the donation of the oxygen lone pairs. Investigations of the reactivity of **MTO** with various substrates have been reported as well but do not specifically pertain to this study.[52−55]

## Computational Methods

Quantum mechanical computations were performed using the B3LYP density functional. This functional is a combination of the hybrid three-parameter Becke exchange functional (B3)[56] and the Lee−Yang−Parr correlation functional (LYP).[57] The basis sets used with B3LYP were constructed as follows. For rhenium we used the core-valence effective core potential of Hay and Wadt,[58] while the Pople-style 6-311G**[59] basis set was utilized for hydrogen, carbon, and oxygen atoms. Since some reactions include negatively charged species, the effects of diffuse functions were included by computing single-point energies with the

(45) Copéret, C.; Adolfsson, H.; Khuong, T. A. V.; Yudin, A. K.; Sharpless, K. B. *J. Org. Chem.* **1998**, *63*, 1740.
(46) Copéret, C.; Adolfsson, H.; Sharpless K. B. *Chem. Commun.* **1997**, *16*, 1565.
(47) Costa, P. J.; Calhorda, M. J.; Bossert, J.; Daniel, C.; Romao, C. C. *Organometallics* **2006**, *25*, 5235.
(48) de Simone, M.; Coreno, M.; Green, J. C.; McGrady, S.; Pritchard, H. *Inorg. Chem.* **2003**, *42*, 1908.
(49) Morris, L. J.; Downs, A. J.; Greene, T. M.; McGrady, G. S.; Hermann, W. A.; Sirsch, P.; Schrer, W.; Gropen, O. *Organometallics* **2001**, *20*, 2344.
(50) Kostlmeier, S.; Haberlen, O. D.; Rosch, N.; Hermann, W. A.; Solouki, B.; Bock, H. *Organometallics* **1996**, *15*, 1872.
(51) Mealli, C.; Lopez, J. A.; Calhorda, M. J.; Romao, C. C.; Hermann, W. A. *Inorg. Chem.* **1994**, *33*, 1139.
(52) Jacob, J.; Espenson, J. H.; Jensen, J. H.; Gordon, M. S. *Organometallics* **1998**, *17*, 1835.
(53) Gisdakis, P.; Rosch, N.; Bencze, É.; Mink, J.; Goncüalves, I. S.; Kühn, F. E. *Eur. J. Inorg. Chem.* **2001**, 981.
(54) Gisdakis, P.; Yudanov, P.; Rosch, N. *Inorg. Chem.* **2001**, *40*, 3755.
(55) di Valentin, C.; Gandolfi, R.; Gisdakis, P.; Rosch, N. *J. Am. Chem. Soc.* **2001**, *123*, 2365.
(56) Becke, A. D. *J. Chem. Phys.* **1993**, *98*, 5648.
(57) Lee, C.; Yang, W.; Parr, R. G. *Phys. Rev. B* **1988**, *37*, 785.
(58) Hay, P. J.; Wadt, W. R. *J. Chem. Phys.* **1985**, *82*, 299.
(59) Krishnan, R.; Binkley, J. S.; Seeger, R.; Pople, J. A. *J. Chem. Phys.* **1980**, *72*, 650.

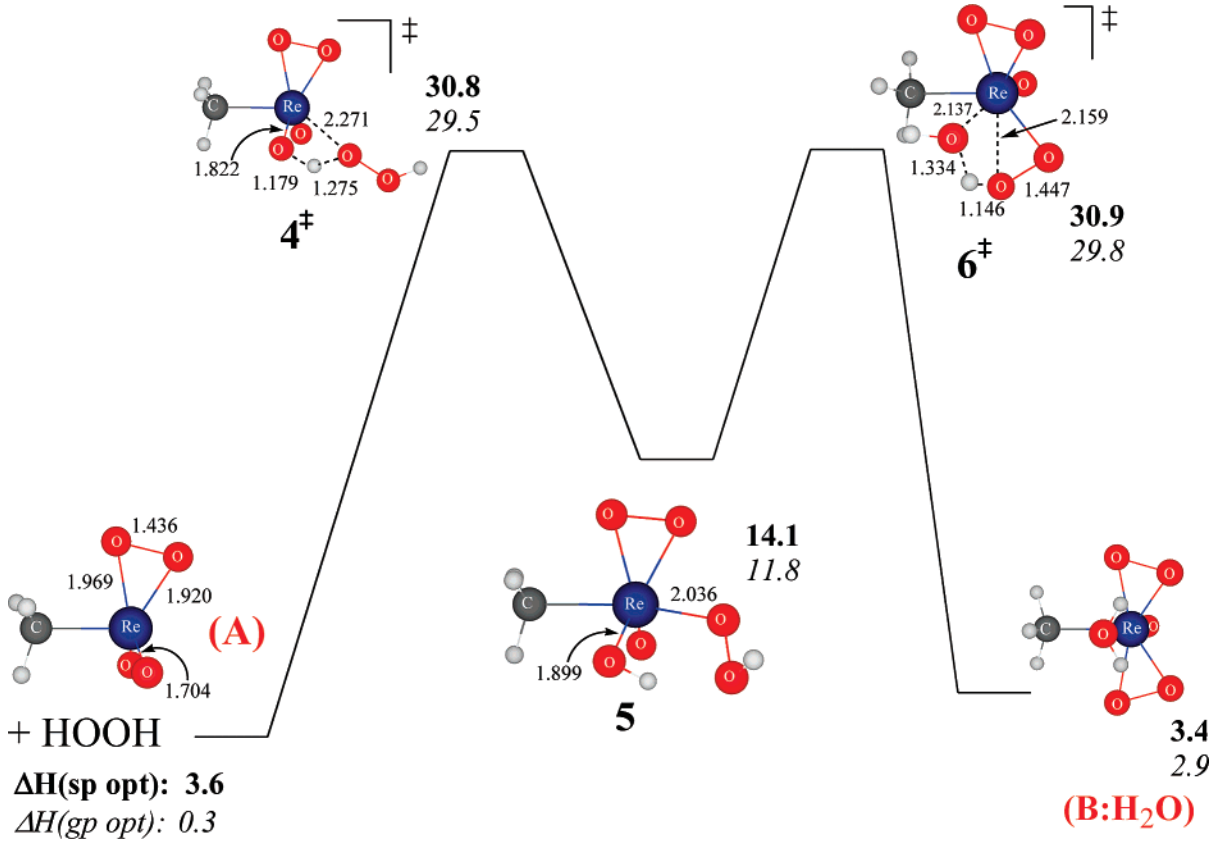


***Figure 3.*** Reaction profile of **A** + $H_2O_2$ → **B:$H_2O$**. The top numbers are enthalpies from solution-phase optimized structures, while the italicized bottom numbers are enthalpies using gas-phase structures with single-point solvation corrections. All energies are with respect to **MTO** and $H_2O_2$ and are listed in kcal $mol^{-1}$, and all distances are listed in Å.

6-311G**++ basis set.[60] All calculations corrected for the effect of solvent interactions by using the polarizable continuum model (PCM) of solvation.[61,62] We solvated with tetrahydrofuran (THF), with a dielectric constant of 7.58 and a probe radius of 2.53 Å. The effect of solvation was computed in two ways: first with a single-point correction for the solvation energy, as was used for the effect of diffuse functions, and second through the calculation of full solution-phase optimized structures.

The generalized valence bond method of Goddard[63] (GVB) was utilized to characterize the orbitals of two key transition states.

The nature of all stationary points was confirmed with a normal-mode analysis, to ensure that minima had zero imaginary frequencies and transition states had exactly one. Solution-phase optimizations were followed by solution-phase frequency calculations (done numerically). In some cases, small imaginary frequencies (less than 40*i*, and always corresponding to methyl rotations) were calculated in solution-phase frequency calculations. These are artifacts of the numerical frequency calculations and can be safely ignored.

The total enthalpies were computed for each stationary point and used for relative enthalpy calculations (at 298.15 K). The final enthalpies were computed as follows, first for the gas-phase optimization:

$$H(\text{GP Opt}) = E^{\text{GP}}_{\text{SCF}} + E^{\text{GP}}_{\text{ZPVE}} + E^{\text{GP}}_{\text{tr}} + E^{\text{GP}}_{\text{rot}} + E^{\text{GP}}_{\text{vib}} + E_{\text{solv}} \quad (1)$$

Note that $E^{GP}_{SCF}$ is the single-point energy computed with diffuse functions at the previously optimized geometry, according to the convention B3LYP/6-311G**++//B3LYP/6-311G**. Additionally, we do NOT include a *PV* term since reactions are in solution phase and *PV* is very small. The enthalpy for the solution-phase optimization is constructed thus:

$$H(\text{SP Opt}) = E^{\text{SP}}_{\text{SCF}} + E^{\text{SP}}_{\text{ZPVE}} + E^{\text{SP}}_{\text{tr}} + E^{\text{SP}}_{\text{rot}} + E^{\text{SP}}_{\text{vib}} + \Delta E_{\text{diff}} \quad (2)$$

The only differences between eqs 1 and 2 are the exclusion of $E_{solv}$ (this term is implicit in $E^{SP}_{SCF}$) and the inclusion of $\Delta E_{diff}$. $\Delta E_{diff}$ is the correction for diffuse functions, that is $E$(B3LYP/6-311G**++) − $E$(B3LYP/6-311G**) at the optimized gas-phase geometry (geometry changes between species in the gas- and solution-phase are very small). Throughout the discussion we focus on the solution-phase optimized enthalpies but include the gas-phase optimized values for comparison. All calculations were computed with the Jaguar 6.0 and Jaguar 6.5 computational packages.[64]

## Results

In order to ensure a complete understanding of the oxygen insertion into the Re−$CH_3$ bond, we elected to explore the entire reaction space for **MTO**, $H_2O_2$, and $OH^-$, which also includes the transformation of **MTO** into the peroxo species **A** and **B** (see Scheme 1). Here, we have kept the naming scheme the same as that by Espenson et al.[26] for ease of discussion.

**Reaction I: MTO + $H_2O_2$ → A + $H_2O$.** The reaction profile for this transformation is shown in Figure 2. The reaction progresses through two distinct transition states, the first (**1**‡)

(60) Clark, T.; Chandrasekhar, J.; Schleyer, P. V. R. *J. Comput. Chem.* **1983**, *4*, 294.
(61) Tannor, D. J.; Marten, B.; Murphy, R.; Friesner, R. A.; Sitkoff, D.; Nicholls, A.; Ringnalda, M.; Goddard, W. A.; Honig, B. *J. Am. Chem. Soc.* **1994**, *116*, 11775.
(62) Marten, B.; Kim, K.; Cortis, C.; Friesner, R. A.; Murphy, R.; Ringnalda, M.; Sitkoff, D.; Honig, B. *J. Phys. Chem.* **1996**, *100*, 9098.
(63) Bobrowicz, F.; Goddard, W. A., III. In *Modern Theoretical Chemistry: Methods of Electronic Structure Theory*; Schaefer, H. F., III, Ed.; Plenum: New York, 1977; Chapter 4.
(64) Jaguar 6.0; J. Schrodinger, LLC: Portland, OR, 2005.

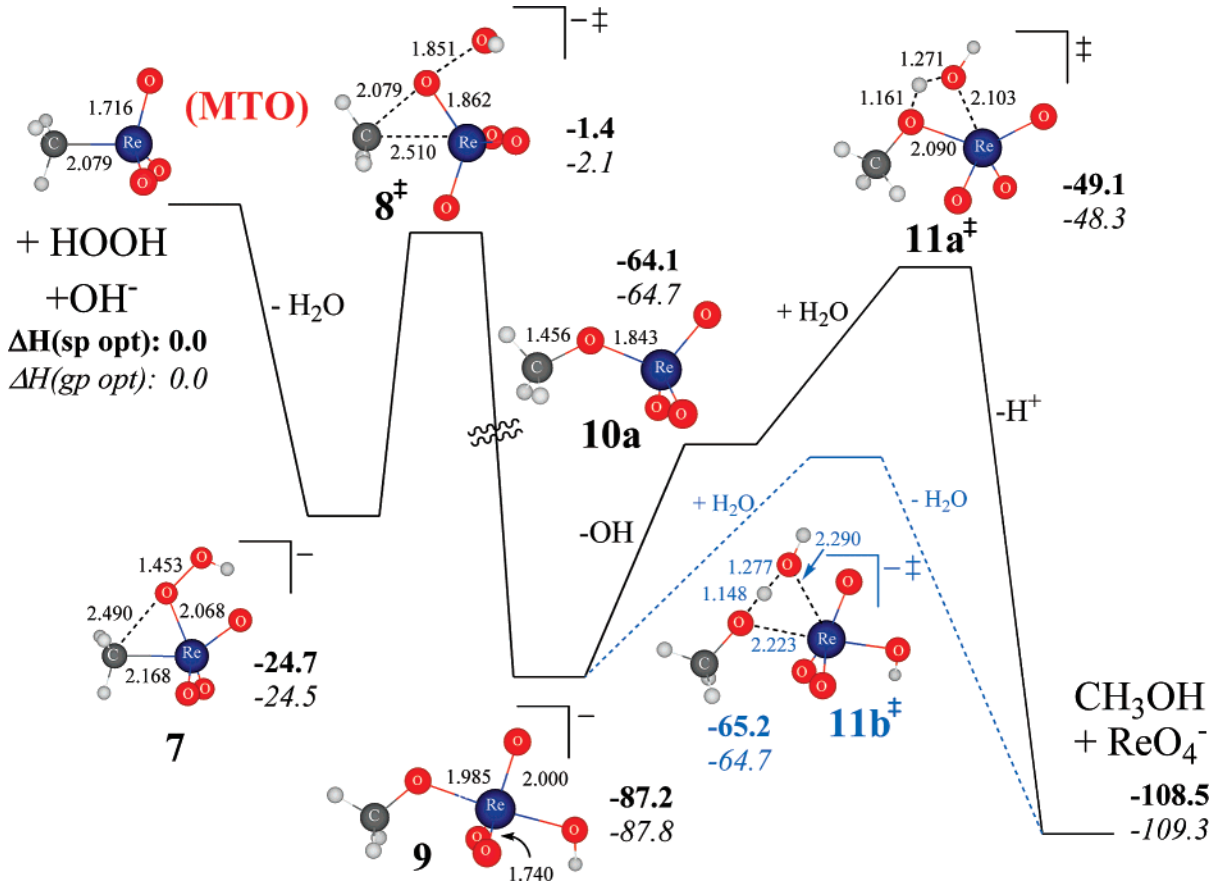


***Figure 4.*** Reaction profile of **MTO** + $OOH^-$ → $CH_3OH$ + $ReO_4^-$. The top numbers are enthalpies from solution-phase optimized structures, while the italicized bottom numbers are enthalpies using gas-phase structures with single-point solvation corrections. All energies are with respect to **MTO** and $H_2O_2$ and are listed in kcal $mol^{-1}$, and all distances are listed in Å. Energies are not shown to scale.

being of higher enthalpy, having a barrier height of 25.0 kcal $mol^{-1}$. Structure **1**‡ can be seen as a hydrogen transfer transition state and, thus, involves the breaking of one of the peroxy O−H bonds while beginning the formation of oxo−hydrogen and rhenium−peroxo bonds. Note that the peroxide attacks the rhenium atom between the rhenium−carbon and one of the rhenium−oxygen bonds, with the dihedral $\tau$(C−Re−O−$O_{peroxy}$) = −22°. For convenience, we label this as a *cis* attack, referring all *cis*/*trans* nomenclature to the Re−$CH_3$ bond. We also explored the possibility of a *trans* attack and found this transition state to be 2.2 kcal $mol^{-1}$ higher in energy than **1**‡**.**

Transition state **1**‡ leads to the stable intermediate **2**, 11.0 kcal $mol^{-1}$ uphill from **MTO**. Species **2** resembles a distorted trigonal bipyramid, where the Re−OH group is angled away from the Re−C bond. This is most likely due to a combination of hydrogen-bond stabilization (between the hydroxyl hydrogen and the bound peroxo oxygen) and a *trans* influence from the methyl group. From **2**, the transformation proceeds through the transition state **3**‡, where the $\beta$-hydrogen is transferred to the hydroxyl group (forming water), while the $\beta$-peroxo oxygen binds to rhenium. Transition state **3**‡ is lower in enthalpy than **1**‡ ($\Delta H_{sp}$ = 21.3 kcal $mol^{-1}$), and the relatively unstable intermediate results in a small relative barrier, 10.3 kcal $mol^{-1}$ with respect to **2**. From **3**‡, it appears that water dissociates completely from the Re before a stable intermediate is formed, leading to direct formation of compound **A**, at a relative (to **MTO**) enthalpy of 3.6 kcal $mol^{-1}$. We did find an **A:$H_2O$** complex that is 0.2 kcal $mol^{-1}$ lower in energy than the separated species (enthalpy), but entropic effects should make **A:$H_2O$** less favorable than the separated species.

**Reaction II: A + $H_2O_2$ → B.** This process (as shown in Figure 3) is similar to what was observed for the previous reaction, with some notable differences. Here the first transition state (**4**‡) is a *trans* attack involving the stretching of a peroxo−hydrogen bond and formation of oxo−hydrogen and rhenium−oxygen bonds. The first barrier is 27.2 kcal $mol^{-1}$ relative to **A** + $H_2O_2$ (30.8 kcal $mol^{-1}$ relative to **MTO**). It should be noted that while this relative barrier is 2.2 kcal $mol^{-1}$ higher than **1**‡, it is exactly the same as that of the *trans* version of **1**‡, suggesting that the peroxy group does not influence the *trans* attack. However, the *cis* transition state has a barrier of 29.3 kcal $mol^{-1}$ relative to **A** + $H_2O_2$, most likely due to the added steric influence of the peroxy group. Transition state **4**‡ leads to the stable intermediate **5**, which is 14.1 kcal $mol^{-1}$ uphill from **MTO**. The second transition state (**6**‡), again a hydrogen transfer, has a relative barrier of 16.8 kcal $mol^{-1}$ from **5**. Species **6**‡ entails a second hydrogen transfer from the peroxy group and a concomitant formation of the second Re−O bond, forming the second $\mu$-peroxo group. The rate-determining transition state is **6**‡, but it has almost the same enthalpy as **4**‡, consistent with their similar structures. The product **B:$H_2O$**, which has one bound water, is roughly thermoneutral with respect to **A**, with a relative enthalpy of 3.4 kcal $mol^{-1}$ with respect to **MTO**. A stable form of **B**, without the bound water, is 8.0 kcal $mol^{-1}$ higher in energy.

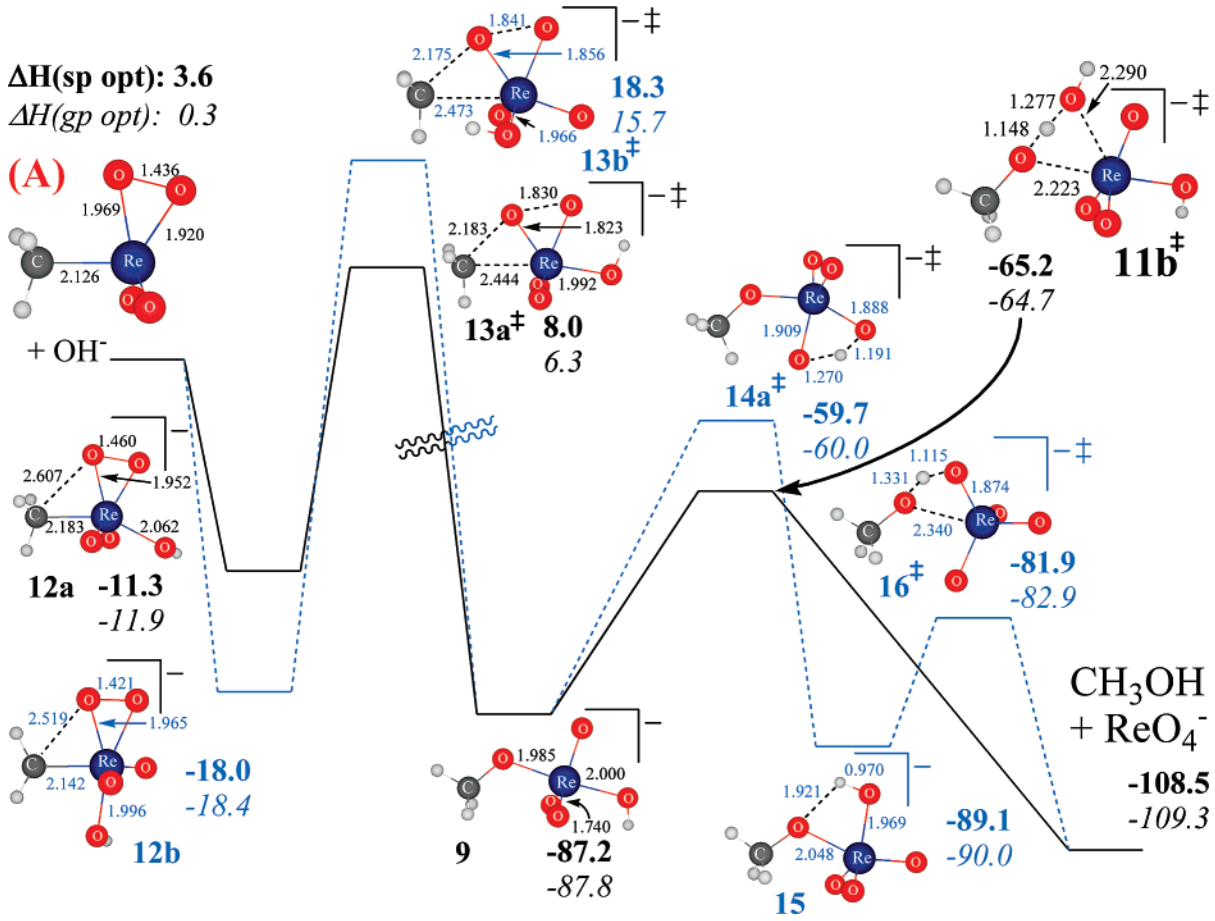


***Figure 5.*** Reaction profile of **A** + $OH^-$ → $CH_3OH$ + $ReO_4^-$. The top numbers are enthalpies from solution-phase optimized structures, while the italicized bottom numbers are enthalpies using gas-phase structures with single-point solvation corrections. All energies are with respect to **MTO** and $H_2O_2$ and are listed in kcal $mol^{-1}$, and all distances are listed in Å. Energies are not shown to scale.

Of immediate concern is the observation that our thermodynamics are potentially not in agreement with previous experimental results,[26,28,30] namely that the formation of **B** should be exothermic with respect to **A** and **MTO** ($\Delta G = -4.2$ kcal $mol^{-1}$ with respect to MTO). Comparing the calculated geometry of **B:$H_2O$** with the X-ray geometry reported by Herrmann and coworkers[65] showed very good agreement for bond lengths (rms deviation = 0.031 Å) and bond angles (rms deviation = 1.9°), except for the length of the Re−$OH_2$ bond ($r_{theoretical}$ = 2.420 Å, $r_{experimental}$ = 2.253(4) Å). However, we noted that Herrmanns X-ray structure of **B:$H_2O$** includes a diglyme molecule that hydrogen bonds to the two hydrogens on $H_2O$, which prompted us to explore the possibility that explicit THF solvent molecules could play a role in Espenson's measured equilibrium.

Indeed, the water moiety in **B:$H_2O$** is capable of interacting strongly with solvent THF molecules, as shown by the following two reactions:

$$\mathbf{B} + H_2O \rightarrow \mathbf{B{:}H_2O} \qquad \Delta E = -7.3 \text{ kcal mol}^{-1} \quad (3)$$

$$\mathbf{B} + H_2O(THF)_2 \rightarrow \mathbf{B{:}H_2O(THF)_2} \qquad \Delta E = -15.0 \text{ kcal mol}^{-1} \quad (4)$$

Thus, the inclusion of explicit solvent molecules stabilizes the **B:$H_2O$** product by 7.7 kcal $mol^{-1}$, relative to the reaction without solvent THF molecules. Subtracting 7.7 kcal $mol^{-1}$ from our relative enthalpy for **B:$H_2O$** (3.4 kcal $mol^{-1}$) yields a final enthalpy of −4.3 kcal $mol^{-1}$, in excellent agreement with the experimental $\Delta G$ of −4.2 kcal $mol^{-1}$. We are thus confident in the technical accuracy of our individual calculations.

However, this did raise the possibility that explicit THF could perturb other aspects of the mechanism. We thus carried out control calculations on the key parts of the mechanism (**MTO**, **A**, **7**, and **8‡**; vide infra for details on **7** and **8‡**). Adding explicit THF to these complexes only changed the relative enthalpy by ±1 kcal $mol^{-1}$, and we thus conclude that THF does not play an active role in the mechanism and can be safely ignored.

**Reaction III: MTO + $OOH^-$ → $CH_3OH$ + $ReO_4^-$ + $H_2O$.** When base is added to a solution of peroxide in THF, $OOH^-$ will form. $OOH^-$ can form three different complexes when bound to **MTO**. The lowest enthalpy conformer (**7**) is shown in Figure 4 and entails a *cis* attack on the metal atom, resulting in a very stable ground state at −24.7 kcal $mol^{-1}$ with respect to the reactants. The two other complexes include another *cis* complex that is similar to **7**, with a rotation along the rhenium−peroxy bond at a relative enthalpy of −21.6 kcal $mol^{-1}$ and a *trans* complex at an enthalpy of −19.9 kcal $mol^{-1}$.

The reaction proceeds through what we term a Baeyer−Villiger type transition state (**8‡**), in which an oxygen is inserted in the carbon−rhenium bond while hydroxide is kicked out as a leaving group, with a relative barrier of 23.3 kcal $mol^{-1}$. Charge is beginning to localize onto the $OH^-$ group, with a net

(65) Herrmann, W. A.; Fischer, R. W.; Scherer, W.; Rauch, M. *Angew. Chem.* **1993**, *105*, 1209; *Angew. Chem., Int. Ed. Engl.* **1993**, *32*, 1157.

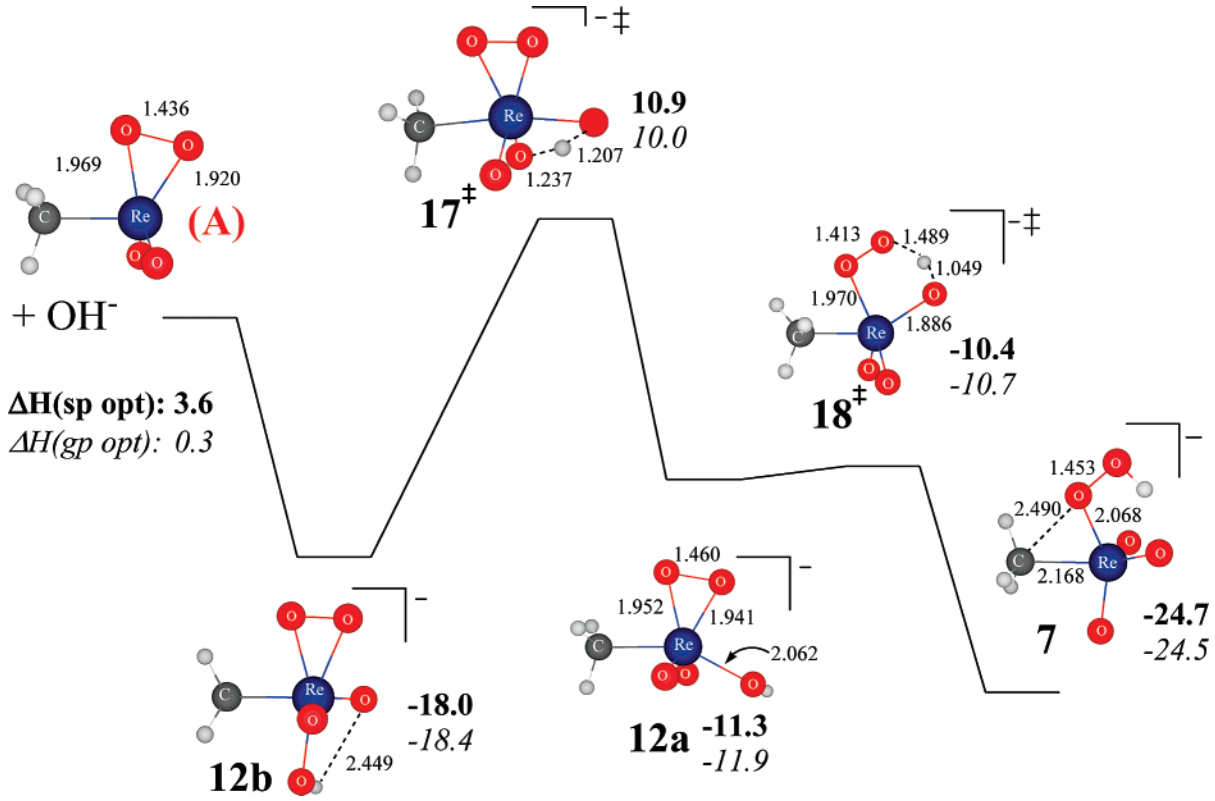


***Figure 6.*** Reaction profile of connection between reaction III and reaction IV via two transition states, **17**‡ and **18**‡. The top numbers are with solution-phase optimized structures. The italicized bottom numbers are the enthalpies using gas-phase structures with single-point solvation corrections. All energies are with respect to **MTO** and $H_2O_2$ and are listed in kcal mol$^{-1}$. All bond distances are in Å.

Mulliken charge increase of 0.2 electrons in the transition state. The Re−C and O−O bonds have been stretched by 0.342 and 0.317 Å, respectively, while the key C−O distance has shrunk by 0.411 Å. Intriguingly, the O−Re distance is 1.862 Å (a decrease of 0.206 Å), a distance roughly equivalent to a conventional O−Re single bond. This is indicative of more bonding than would be expected in a transition state, where bonds are typically partially formed.

From **8**‡, the structure descends dramatically downhill to the intermediate methoxy species **9**, with a relative enthalpy of −87.2 kcal mol$^{-1}$. Note that the O−Re distance in **9** is actually *longer* than that in the transition state **8**‡, by 0.107 Å. This is possibly caused by the presence of the hydroxide trans to the methoxy group, which could prevent the methoxy oxygen from forming a full single bond.

From **9**, the reaction can proceed in several ways. One possible mechanism progresses by dissociation of OH$^-$, with a cost of 23.1 kcal mol$^{-1}$, leading to **10a**. Hydrolysis of **10a** results in the final formation of methanol and perrhenic acid via transition state **11a**‡, with a relative barrier of 15.0 kcal mol$^{-1}$, i.e. 38.1 kcal mol$^{-1}$ higher in energy than **9**. A second possible mechanism is direct hydrolysis via transition state **11b**‡, with a relative barrier of 22.0 kcal mol$^{-1}$. Both of these hydrolysis reactions are similar to a type of mechanism we recently characterized as internal electrophilic substitution (IES).[66] The IES transition state is similar in structure to a sigma-bond metathesis (SBM) transition state but, unlike SBM, utilizes the lone pair on the accepting heteroatom to abstract the hydrogen. The O:Re coordination is transformed into an O—Re bond, while the Re═O is simultaneously transformed into a Re—OH bond, making it a six-electron process. The metal acts as an electrophile, which in turn activates the hydrogen toward attack by the electrophilic lone pair. A third mechanism, featuring a hydrogen transfer from the hydroxyl group in **9** to one of the oxo groups, is also possible and is discussed in the next section.

In addition, we explored the possibility of **7** reacting directly to form the $\mu$-peroxo species **A**. We could not find a direct pathway that would form **A** but were able to find a transition state that transferred a hydrogen from the peroxo group of **7** to the *trans* oxo group, forming an **A:OH**$^-$ compound, with the hydroxyl *trans* to the methyl. This process has a barrier of only 14.3 kcal mol$^{-1}$ and is discussed in a subsequent section (see transition state **18**‡).

We also explored the possibility of a direct elimination reaction, in which the $\beta$-oxygen of the OOH group forms a bond with the methyl group while methanol leaves. However, this has a very high relative barrier of 50.9 kcal mol$^{-1}$ (with the smaller 6-31G** basis set) and was not further pursued. Furthermore, we explored the reactive chemistry of the **MTO:OH**$^-$ species and found it had very similar trends to **MTO**, but the ground state OOH$^-$ adduct was at a much higher enthalpy (−15 kcal mol$^{-1}$ compared to −25 kcal mol$^{-1}$ for the **MTO:OOH**$^-$ adduct, **7**) and is consequently not further discussed.

**Reaction IV: A + OH$^-$ → MeOH + ReO$_4^-$ + H$_2$O.** In addition to the reaction of **MTO** with OOH$^-$, we must also consider the reaction of **A** with OH$^-$. The simplest possibility is a direct $S_N2$ attack on the $sp^3$ carbon. We carefully explored the potential energy surface for just such a transition state to

(66) Oxgaard, J.; Tenn, W. J., III; Nielsen, R. J.; Periana, R. A.; Goddard, W. A., III. *Organometallics* **2007**, *26*, 1565.

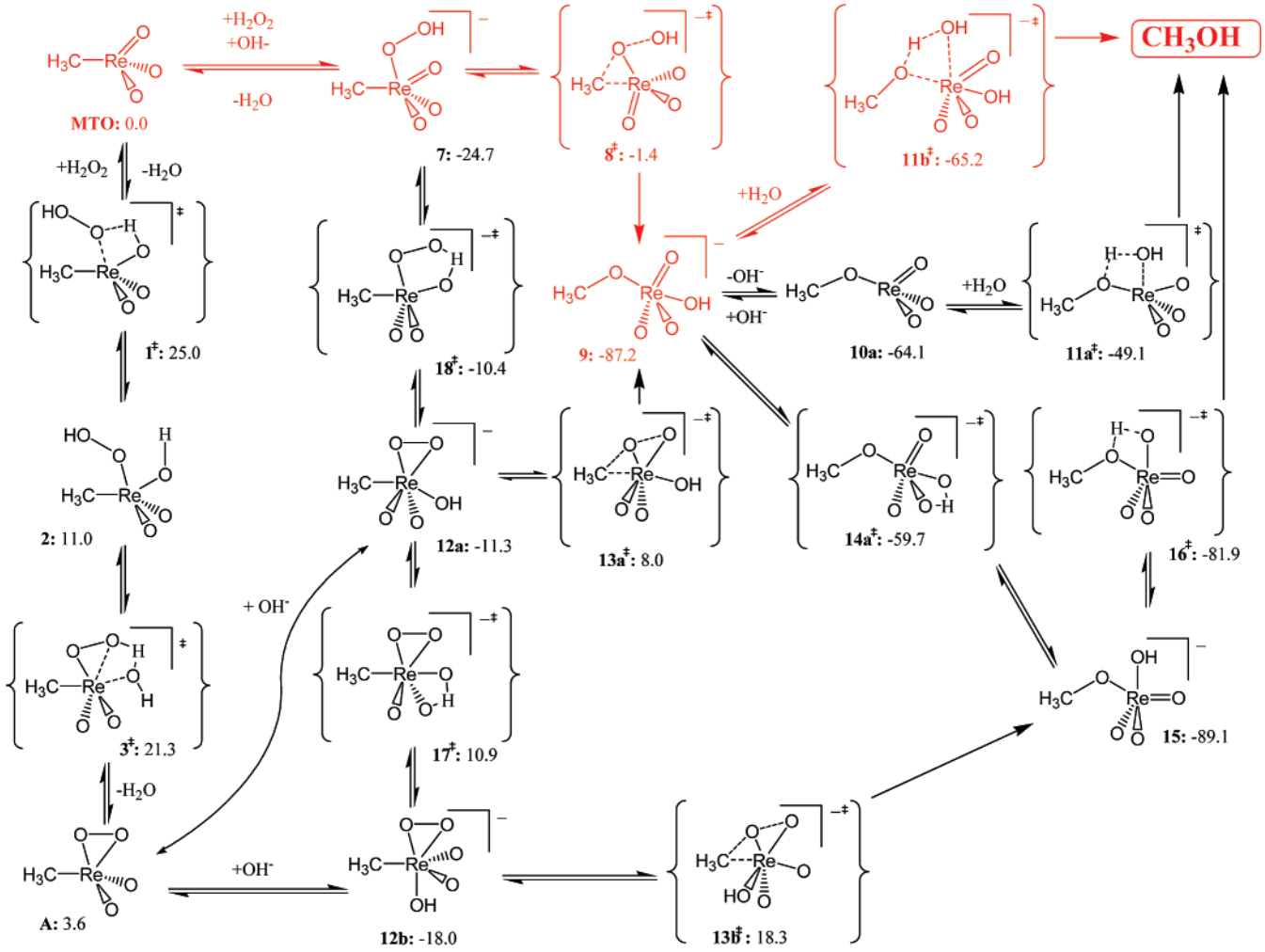


***Figure 7.*** Schematic of reaction progression to form methanol from **MTO**, $H_2O_2$, and $OH^-$. All energies are from the solution optimized calculations and are in kcal $mol^{-1}$. The red path is the lowest energy pathway for the formation of methanol.

no avail. Instead, we explored the possibility of stepwise reactions. **A** can form three different complexes with $OH^-$, two of which are shown in Figure 5, **12a** and **12b**. The lowest energy complex, **12b** (at −18.0 kcal $mol^{-1}$), has hydroxide complexed *cis* to the methyl group, while the higher energy species **12a** (at −11.3 kcal $mol^{-1}$) has the hydroxide *trans* to the complex. A third complex, which has the hydroxide *cis* to both the methyl and peroxo groups, has a relative energy of −13.8 kcal $mol^{-1}$ but reacts similarly to **12b** and is not illustrated. Similarly to **9**, we explored the possibility of direct reductive elimination of $CH_3OH$ from **12b**, but this has a relative barrier of 46.5 kcal $mol^{-1}$ (using the smaller 6-31G** basis set) and is thus not viable.

Both **12a** and **12b** can react via formation of a carbon−peroxo bond with a concerted break of the peroxo−peroxo and carbon−rhenium bond, as seen in transition states **13a**‡ and **13b**‡. Both **13a**‡ and **13b**‡ are concerted transition states, with the C−Re and O−O bonds stretching, and the C−O bond forming. Note that **13b**‡ is much higher in energy, with an effective barrier of 36.3 kcal $mol^{-1}$, while **13a**‡ is an accessible transition state with a barrier of only 19.3 kcal $mol^{-1}$. Similar to what we saw in **8**‡, the Re−O bond decreases in length in the transition state, by 0.121 Å for **13a**‡ and 0.099 Å for **13b**‡. In addition to the shorter (and thus stronger) Re−O bond, the C−Re and O−O bonds are less stretched in **13a**‡ than **13b**‡, partially explaining the lower relative enthalpy.

Transition states **13a**‡ and **13b**‡ are superficially dissimilar from **8**‡, in that there is no leaving group formed. However, one could consider the forming Re−$O^-$ the equivalent of $HO^-$ and thus as an internal leaving group. Consequently, we believe that the three transition states are related in type and behavior, as further elaborated in the discussion.

Both reactions progress downhill to stable methoxy intermediates (**9** and **15**, respectively) in which the carbon−oxygen bond has been fully formed. Some of the product formation from **9** was discussed in the section on Reaction III, where we showed that **9** can either dissociate $OH^-$ and hydrolyze (**11a**‡) or directly hydrolyze (**11b**‡) to form methanol. In addition, **9** can convert to **15** through hydrogen transfer between the Re−OH group and one of the Re=O oxygens (transition state **14a**‡), followed by a series of rotations around the Re−OH and Re−$OCH_3$ bonds (not shown). The calculated energy of **14a**‡ is −60.0 kcal $mol^{-1}$, leading to a relative barrier of 27.5 kcal $mol^{-1}$. Intermediate **15** can convert to methanol and the perrhenate anion through a simple hydrogen transfer from the −OH group to the methoxy moiety (via transition state **16**‡), with a relative barrier of only 8.0 kcal $mol^{-1}$. While this is

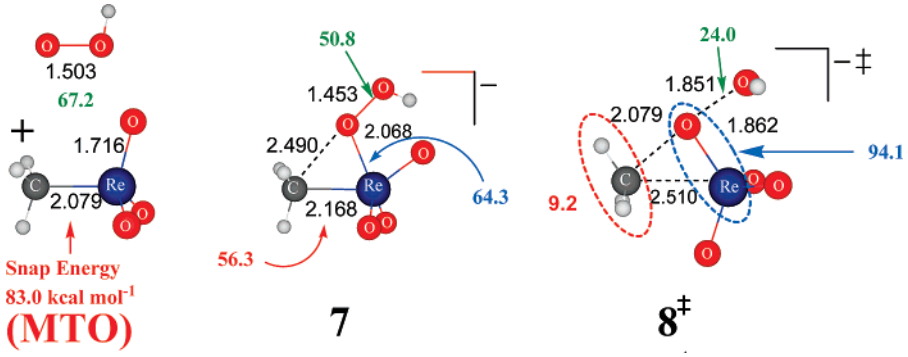


***Figure 8.*** Schematic of homolytic bond and fragment energies for **MTO**, $OOH^-$, **7**, and **8**‡.

significantly lower than the relative barrier for product formation through **11b**‡ (22.0 kcal $mol^{-1}$), the relative barrier of 27.5 kcal $mol^{-1}$ for formation of **15** from **14a**‡ is a few kcal $mol^{-1}$ higher. Furthermore, the high enthalpy of **13b**‡ precludes formation of **15** from forming directly from **12b**. The large difference in barriers between the three hydrogen transfer steps **14a**‡, **16**‡, and **11b**‡ is most likely due to the difference in exothermicity, namely **9** → **15** is almost thermoneutral, while **15** → $CH_3OH$ + $ReO_4^-$ is downhill by 19.4 kcal $mol^{-1}$, and the relative barriers reflect this according to the Hammond postulate.

**Connecting Intermediates from Reaction III and Reaction IV.** Careful examination of the intermediates in reactions III and IV indicates that several of the intermediates can interconvert into each other. For example, the complexes **12a** and **12b** can interconvert through transition state **17**‡, as shown in Figure 6. Transition state **17**‡ is a hydrogen transfer between a hydroxyl and an oxo group and has a relative barrier height of 28.9 kcal $mol^{-1}$, consistent with what was seen for **14a**‡. While this barrier is 7.6 kcal $mol^{-1}$ higher in enthalpy than simply dissociating the hydroxyl anion from **12b** and reassociating to form **12a**, it could have implications for experimental labeling studies.

More important is the possibility that **7** can convert to **12a**, through transition state **18**‡, with a calculated relative barrier of only 14.3 kcal $mol^{-1}$. This transition state is a hydrogen transfer from the peroxy group to one of the oxo groups. Complex **12a** can in turn functionalize the C−Re bond with a small relative barrier of 19.3 kcal $mol^{-1}$, as seen in reaction IV. This leads to an indirect pathway for the formation of **A** from **MTO** with a net barrier lower than that seen in **1**‡.

## Discussion

With the multiple mechanisms presented in this report, it is necessary to compare all possible steps and how they interconnect. Because many paths go through intermediate **9**, we will not list them all but rather focus on the most important ones. Figure 7 schematically presents several of the mechanisms explicitly shown in Figures 4−6, with the reaction path of lowest barrier on the top, in red. The most facile reaction is thus the path highlighted in reaction III, namely **MTO** → **7** → **8**‡ → **9** → **11b**‡ → **$CH_3OH$**, with the rate-determining step being the Baeyer−Villiger type transition state, **8**‡, with a net reaction barrier of 23.3 kcal $mol^{-1}$. Several other pathways were explored, but since we find that the resting state of MTO + $OH^-/H_2O_2$ is **7**, no other pathway is able to compete with **8**‡. It should be noted that in our previous communication on this mechanism[30] we found a barrier of 18 kcal/mol for the $\mu$-peroxo mechanism (see Figure 1). We now find that this barrier is only relative, and the absolute barrier for $\mu$-peroxo insertion is 32.7 kcal/mol.

While the overall mechanism is interesting, the primary motivation for this work is to understand *why the barrier for C−O coupling is so low*. We have characterized two pathways for oxygen insertion into the Re−C bond with relative barriers under 24 kcal $mol^{-1}$ (through **8**‡ and **13a**‡), and as they appear to be related, we will concentrate our analysis to **8**‡.

In **MTO**, the computed homolytic energy of the Re−$CH_3$ bond is 83 kcal $mol^{-1}$, while the O−OH homolytic bond strength is 67.2 kcal $mol^{-1}$ (see Figure 8).[67] Intriguingly, when $^-$OOH complexes to **MTO** to form **7**, the Re−$CH_3$ bond strength decreases to 56.3 kcal $mol^{-1}$, while the O−OH bond decreases to 50.8 kcal $mol^{-1}$. This is compensated for by the formation of a Re−OOH bond worth 64.3 kcal $mol^{-1}$, as well as a significantly changed solvation energy (not shown). It is not clear how important the destabilization of the Re−$CH_3$ and O−OH bonds is, but it seems reasonable that it will lower the barrier of the transition state where both of these bonds are broken.

In the transition state, **8**‡, the presence of multiple atomic interactions complicates the assignment of bond strengths. However, the long C−O distance of 2.08 Å suggests that this interaction should be minimal, an assertion supported by the interaction energy of merely 9.2 kcal $mol^{-1}$ for the methyl fragment.[68] Furthermore, the summed Mulliken charges on the methyl fragment are approximately zero, implying that the methyl fragment can be considered a radical, consistent with the concerted heterolytic C−Re bond cleavage and concomitant C−O and O−Re bond formations. The small interaction energy of the methyl moiety also suggests that the Re−$CH_3$ bond is almost completely broken in the transition state. Furthermore, the O−OH bond is now reduced to 24.0 kcal/mol, i.e., less than half that of the bond in the free $^-$OOH anion. However, the Re−OOH homolytic bond energy[67] is calculated to be 94.1 kcal $mol^{-1}$, i.e., almost 30 kcal $mol^{-1}$ *stronger* than that in **7**. Even if some of this interaction is due to O−C bonding, it is clear that the Re−OOH bond is substantially stronger in **8**‡ than in

(67) Homolytic bond energies are evaluated by computing the relative energy of the two fragments relative to the entire molecule. Note that the fragment geometries are frozen in the exact same structure as they exhibit in the full molecule.

(68) The 9.2 kcal $mol^{-1}$ was computed as discussed in ref 67, with the two species being the methyl radical fragment and $ReO_3(OOH)-$ being the radical fragment. Other fragment energies were computed similarly.

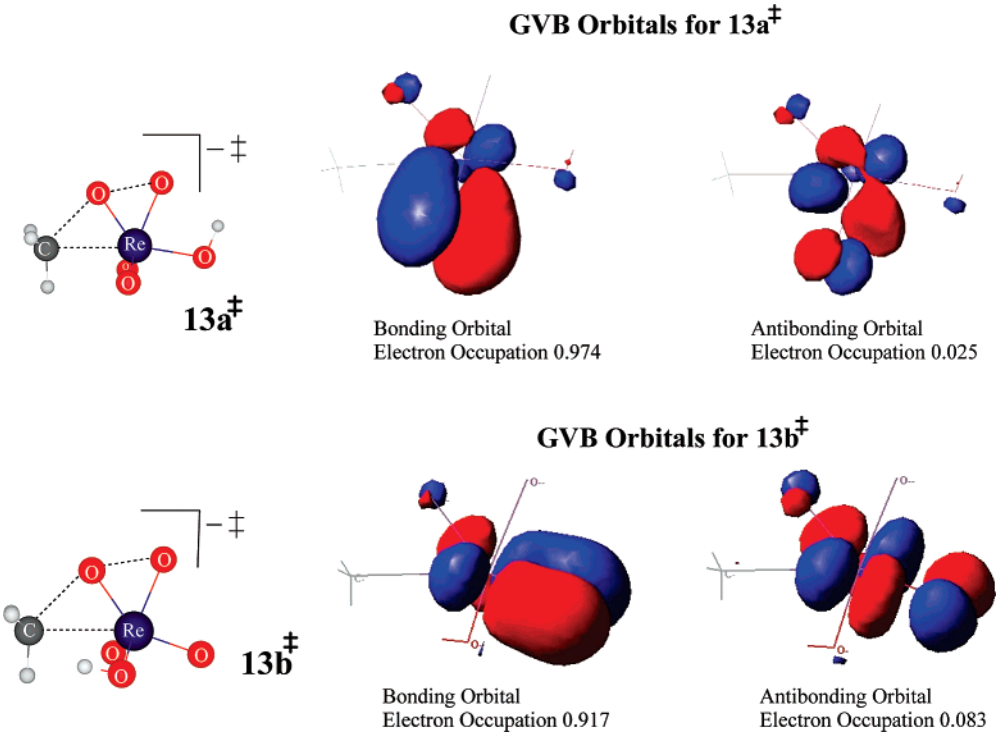


***Figure 9.*** Key GVB orbitals for transition states **13a**‡ and **13b**‡.

**7**, which we believe is the cause of the relatively low enthalpy of the transition state.

The key to this chemistry thus appears to be the ability of the oxygen to form a very strong Re−O interaction early on in the mechanism, which offsets the loss of Re−C bond energy. Furthermore, it seems likely that the electron density in the Re−C bond is actively being donated to *both* the Re−O and O−O bonds, stabilizing the transition state through the formation of the Re−O bond while the O−O bond is broken. An alternative way of looking at this is that coordinating the $^-$OOH anion renders the methyl group in **7** significantly more negatively charged (thus more nucleophilic) and the OOH fragment less negative (thus more electrophilic), which should improve the barrier for oxidation, since this requires the transfer of electrons from the reducant to the oxidant. Nevertheless, the key aspect is that the electron density that was donated from $^-$OOH *must* transfer to the $-CH_3$ moiety.

Consequently, the $d^0$ nature of the Re(VII) system does appear to be integral for this chemistry. If an occupied d-orbital is available, it would most likely donate into the M−O bond before the M−C bond is broken, generating an inert M=O moiety. Indeed, preliminary calculations on a Baeyer−Villiger type insertion with **MDO** ($CH_3$−$ReO_2$), a $Re^V$ complex, suggest that formation of **MTO** is significantly more favorable than C−Re insertion. However, there is a possibility that if a system can be found where the energy of the highest occupied d-orbital is lower in energy than the M−C bond, it could be possible to enable this chemistry. For example, it is conceivable that a system based on a $Ir^V$, $Pt^{IV}$, or even $Pt^{II}$ could be competent for this, although not necessarily with $^-$OOH. (We have in our previous work demonstrated how other oxidants, such as $IO_4^-$ and PhIO, are capable of performing the same chemistry as $^-$OOH.[30]) For design purposes, it should also be noted that the current mechanistic interpretation requires a vacant coordination site where the $O^-$ can complex or the stabilizing M−O bond cannot form. These assumptions and predictions are currently being computationally tested.

One more observation from our results warrants further inspection, namely the surprisingly high energy of transition state **13b**‡, as compared to **13a**‡. **13b**‡ has a relative barrier of 36.3 kcal mol$^{-1}$, while **13a**‡ has a relative barrier of merely 19.3 kcal mol$^{-1}$, yet a superficial analysis of the geometry of the reacting atoms in these two transition states show no major differences. This appears to contradict our above analysis, since if the barrier is dependent on the bonds of the reacting atoms, **13a**‡ and **13b**‡ should have the same barrier. However, inspection of the generalized valence bond (GVB) orbitals shows that **13b**‡ takes some electron density out of a Re−O d-$\pi$-bonding orbital and puts it into an antibonding orbital, as shown in Figure 9, with an orbital coefficient of 0.083. In contrast, **13a**‡ has an antibonding orbital with a orbital occupation coefficient of only 0.025, i.e., practically negligible. Why **13b**‡ requires electron density in an antibonding orbital is currently unclear, but the immediate effect is to render the energy of **13b**‡ significantly higher than that of **13a**‡.

## Summary

We have characterized the complex set of interactions between **MTO**, $H_2O_2$, and $OH^-$ and conclude that methanol is formed through a Baeyer−Villiger type mechanism with a net barrier of 23.3 kcal mol$^{-1}$ (**8**‡). Additionally, we isolated another oxygen insertion transition state (**13a**‡) with a low relative barrier (below 24 kcal mol$^{-1}$), which after analysis appears similar to **8**‡. Both these transition states rely on an electrophilic nature and a lack of accessible d-orbitals on the central rhenium. The key to the low barriers is the donation of the electron density from the Re−C bond to *both the forming Re−O and breaking O−O bonds*, simultaneously, thus forming the Re−O bond as

the Re−C bond is broken. These two transition states serve as "concept" models for facile, room-temperature functionalization of metal−carbon bonds, and will be used as models for future attempts in catalysis design. Additional transition metal systems featuring electrophilic centers with low-energy d-orbitals, such as $Pt^{IV}$, pose intriguing possibilities for further development of nonredox catalytic conversion of hydrocarbons.

**Acknowledgment.** Support of this work was provided by the DOE (EERE-DE-PS36-06GO096018-3A). The facilities of the Materials and Process Simulation Center used for these studies were provided by DURIP-ARO and DURIP-ONR. The authors thank the Chevron-Texaco Energy Research and Technology Company for financial support for this research.

**Supporting Information Available:** The Cartesian coordinates, absolute enthalpies, and solvation energies of all species indicated in the text. This material is available free of charge via the Internet at http://pubs.acs.org.

JA0714742